International Journal of Applied Earth Observation and Geoinformation 21 (2013) 326–340

Contents lists available at SciVerse ScienceDirect

International Journal of Applied Earth Observation and Geoinformation

journal homepage: www.elsevier.com/locate/jag

Exploratory spatial data analysis of global MODIS active fire data

D. Oom*, J.M.C. Pereira

Forest Research Centre, School of Agriculture, Technical University of Lisbon, Tapada da Ajuda 1349-017 Lisboa, Portugal

ARTICLE INFO

Article history:
Received 13 April 2012
Accepted 27 July 2012

Keywords:
Spatial data analysis
Vegetation fires
Global
MODIS

ABSTRACT

We performed an exploratory spatial data analysis (ESDA) of autocorrelation patterns in the NASA MODIS MCD14ML Collection 5 active fire dataset, for the period 2001–2009, at the global scale. The dataset was screened, resulting in an annual rate of false alarms and non-vegetation fires ranging from a minimum of 3.1% in 2003 to a maximum of 4.4% in 2001. Hot bare soils and gas flares were the major sources of false alarms and non-vegetation fires. The data were aggregated at 0.5° resolution for the global and local spatial autocorrelation Fire counts were found to be positively correlated up to distances of around 200 km, and negatively for larger distances. A value of 0.80 ($p = 0.001$, $\alpha = 0.05$) for Moran's I indicates strong spatial autocorrelation between fires at global scale, with 60% of all cells displaying significant positive or negative spatial correlation. Different types of spatial autocorrelation were mapped and regression diagnostics allowed for the identification of spatial outlier cells, with fire counts much higher or lower than expected, considering their spatial context.

1. Introduction

Vegetation fires occur worldwide, at different times of the year and inject large amounts of trace gases and particles into the atmosphere, having important environmental and climatic impact at global, regional and local scales. A reliable classification and characterization of the fire geography and seasonality at global scale that includes inter-annual variations is very important, not only to reduce uncertainties in estimates of emissions from biomass burning, but also to elucidate relationships between large scale climatic phenomena and fire occurrence and distribution at global scale. The use of satellite remote sensing allows for the collection of global, consistent fire information (Csiszar et al., 2005; Dwyer et al., 2000).

During the last decades several global fire analyses used different sensors and algorithms. Dwyer et al. (2000) and Stroppiana et al. (2000) analyzed the global spatial and temporal distribution of 12 months of Advanced Very High Resolution Radiometer (AVHRR) data at 1 km spatial resolution. Prins and Menzel (1992) used data from the Geostationary Operations Environmental Satellite (GOES) at 4 km spatial resolution to study fire activity in the western hemisphere. After that, the European Space Agency (ESA) Along Track Scanning Radiometer (ATSR) World Fire Atlas (WFA) (Arino and Rosaz, 1999; Arino et al., 2005), the NASA/Japan Aerospace Exploration Agency (JAXA) Tropical Rainfall Measuring Mission (TRMM) Visible and Infrared Scanner (VIS) (Giglio et al., 2000), and the active fire product from the Moderate Resolution Imaging Spectroradiometer (MODIS) (Justice et al., 2002) were some of the products that provided a good indication of the distribution of the burned area and active fires at different scales and years. These datasets were used to estimate atmospheric emissions of trace gases (Duncan et al., 2003; Schultz, 2002) and burned area (Eva and Lambin, 1998; Kasischke et al., 2003; Pereira, 2003; Pereira et al., 2004). Nevertheless, some of these products have known limitations. The assumption that the WFA contained few commission errors was disproved by Mota et al. (2006) and Oom (2008). They developed a data screening methodology, which led to the removal of about 25% of WFA observations, not corresponding to vegetation fires. NASA is also developing a global active fires dataset starting in 2000, based on the Aqua and Terra sensors (Giglio et al., 2003). Due to the improved specifications of those sensors for fire detection, four daily overpasses and the use of a more sophisticated detection algorithm this data set is expected to provide a more accurate depiction of global fire. However, the product is not error-free. Local and temporal limited validations of the MODIS active fire product were performed by Giglio et al. (2003, 2006), Morisette et al. (2005a, 2005b), Csissar et al. (2005), Schroeder et al. (2008a, 2008b), De Klerk (2008) and Hawbaker et al. (2008). They reported commission errors in the range of 2–3% (Boschetti et al., 2010). Nevertheless, no quantitative assessment of the MODIS global active fire dataset has been performed so far.

Exploratory data analysis (EDA) is of a set of descriptive and graphical statistical tools designed to find patterns in data and suggest hypotheses by imposing as little prior structure as possible

* Corresponding author. Tel.: +351 21 3653387; fax: +351 21 3653338.
E-mail addresses: duarteoom@isa.utl.pt, duarte.oom@gmail.com (D. Oom), jmcpereira@isa.utl.pt (J.M.C. Pereira).

0303-2434/$ – see front matter © 2012 Elsevier B.V. All rights reserved.
http://dx.doi.org/10.1016/j.jag.2012.07.018

(Tukey, 1977). This leads to "potentially explicable patterns" (Good, 1983), which may originate formal hypotheses and theoretical concepts. Objectives of EDA are to suggest hypotheses concerning the causes of observed patterns, to assess assumptions which underlie statistical inference, and to support the choice of correct statistical methods for the problem under analysis. Exploratory spatial data analysis (ESDA) is an extension of EDA to deal with spatial datasets. It involves specific techniques for detecting spatial patterns in data, formulating hypotheses based on the geography of the data, and assessing spatial models (Haining, 1993). A central concept of ESDA is spatial autocorrelation, the propensity for observations in geographical proximity to have similar values. Global spatial autocorrelation quantifies overall clustering of similar values and is tested against a null hypothesis of random location. Rejection of the null is indicative of spatial patterning in the data, providing useful information concerning the process under study. However, tests for global spatial autocorrelation only assess overall clustering and do not inform on the type (correlation between high values or between low values), extent, and location of spatial clusters and outliers (Anselin, 1995). A more detailed exploration of the data is possible with local indicators of spatial autocorrelation (LISA), which allow assessing the significance of local spatial patterns and classifying them into four types of association, distinguishing local clusters (high–high or low–low) or local spatial outliers (high–low or low–high) (Anselin, 1995). A map showing locations with significant Local Moran statistics, classified by type of spatial correlation is referred to as a LISA cluster map. Some studies have applied these techniques to spatial fire data. Pereira et al. (1998) identified spatial autocorrelation patterns in burned areas for Portugal, based on global and local indicators of spatial association. Chou et al. (1993) incorporated fire occurrence neighborhood effects on a spatial regression model for the San Jacinto Mountains, California, after data analysis based on Moran's *I*. Siljander (2009) modeled fire probability in Namibia using logistic regression. Moran's *I* analysis led to the incorporation of an autocovariate explanatory variable, accounting for neighborhood effects on fire incidence. Morisette et al. (2005a) used Moran's *I* to characterize the spatial patterns of active fires detected with high spatial resolution ASTER imagery, within lower resolution MODIS pixels, while validating MODIS active fire maps for southern Africa. In a fire severity assessment based on ASTER data, Coluzzi et al. (2010) used several spatial autocorrelation statistics to measure and analyze dependency among spectral features of areas burned in southern Italy. Finally, a procedure to detect active fires as spatial outliers in MODIS thermal imagery using Moran scatterplot analysis was proposed by Byun et al. (2006).

The aim of the present work is to perform an ESDA of the active fire data from the Moderate Resolution Imaging Spectrometer (MODIS) MCD14ML product (Justice et al., 2002) for the period 2001–2009 and spatially aggregated at 0.5° cell resolution, using the local Moran's *I* and the Moran scatterplot. The analysis may help identify relevant covariates, deal with model specification issues, such as the identification of spatial regimes, with potentially distinct parameter values, assess the prevalence and importance of local pockets of spatial non-stationarity that may behave as outliers and other influential observations, and assess the pertinence of incorporating a spatially lagged independent variable in the specification of spatial regression models, to be developed in a subsequent study

ESDA results are also relevant to assist in model specification for various types of regression modeling approaches, namely generalized additive modeling (Krawchuk et al., 2009), regression trees (Archibald et al., 2009), spatial hierarchical Bayesian modeling (Amaral-Turkman et al., 2010) and geographically weighted regression (Sá et al., 2011). However none of these studies was preceded by an ESDA.

2. Materials and methods

2.1. Data

The dataset consists of 9 years (January 2001–December 2009) of the MCD14ML Collection 5 active fire product (Justice et al., 2002), obtained with data acquired by the Moderate Resolution Imaging Spectroradiometer (MODIS) on board NASA's Earth Observing System (EOS) Terra (since February 24, 2000) and Aqua satellite (since May 4, 2002). MODIS has spectral and radiometric specifications designed for fire observation, with a spatial resolution of 1 km at nadir. Fire detection is accomplished using a contextual algorithm that exploits the strong emission of mid-infrared radiation from fires and is based on brightness temperatures derived from the 4 and 11 μm channels (Giglio et al., 2003), enhancing the sensitivity to smaller, cooler fires and decreasing the occurrence of false alarms. There are some periods with missing data, from June 16th to July 2nd (2001), March 20th to 27th and April 15th (2002). Although our analysis was performed at 0.5° spatial resolution, the decision of not using the Climate Model Grid (CMG) Fire Products (MOD14CMH, MYD14CMH) was due to our interest in screening daily, individual fire observations in the MODIS products.

We used the same ancillary dataset in the screening procedure as Mota et al. (2006), with updated versions: (i) Global Land Cover 2000 (GLC2000) map (Fritz et al., 2003), which is based on SPOT-VEGETATION 1 km satellite imagery for the year 2000; (ii) a 2008 annual global composite of stable nighttime lights (Elvidge et al., 2001) and an independent gas flare mask (2007) from the Version 4 Defense Meteorological Satellite Program (DMSP) Operational Linescan System (OLS) Nighttime lights time series data (http://www.ngdc.noaa.gov/dmsp/index.html); (iii) volcanic activity timing and location data (2001–2009) from the Global Volcanism Program (GVP) (http://www.volcano.si.edu/), Volcano World (http://http://volcano.oregonstate.edu/) and MODVOLC (http://modis.higp.hawaii.edu/). The terminology used by Mota et al. (2006) was also adopted: MODIS observations are the original fire counts, false alarms are observations that do not correspond to fires (hot ground surfaces or calibration errors) and fires are observations associated with combustion process (including vegetation fires and also non-vegetation fires, such as gas flares and volcanic eruptions (Fig. 1)).

2.2. Methodology

2.2.1. Screening procedure

The screening procedure of Mota et al. (2006) and Oom (2008) applied to the MCD14ML Collection 5 product was implemented in two stages (Fig. 1). In the first stage, spatial masks were applied to remove false alarms generated by hot bare ground and nightlights, as well as non-vegetation fires due to gas flares and volcanic activity. In the second screening stage the data were visually inspected and quantitatively analyzed to search for potential erroneous observations missed in the first stage. These inspections were accomplished calculating the difference between daily observation counts and five-day moving averages and, after aggregating to a 0.5° grid cell (fire counts per cell), the application of Local Moran (I_i) spatial index (Anselin, 1995). Based on the findings of Mota et al. (2006), deserts and sparsely vegetated regions were subject to particularly careful analysis, to identify commission errors. Throughout this second stage the observations excluded are considered false alarms, since they not correspond to combustion processes. The two-stage classification of MODIS observations is exhaustive, i.e. it addresses each and every fire count in dataset, but it is not mutually exclusive, i.e., a given observation may be captured by more than one filter. The goal of the screening is remove

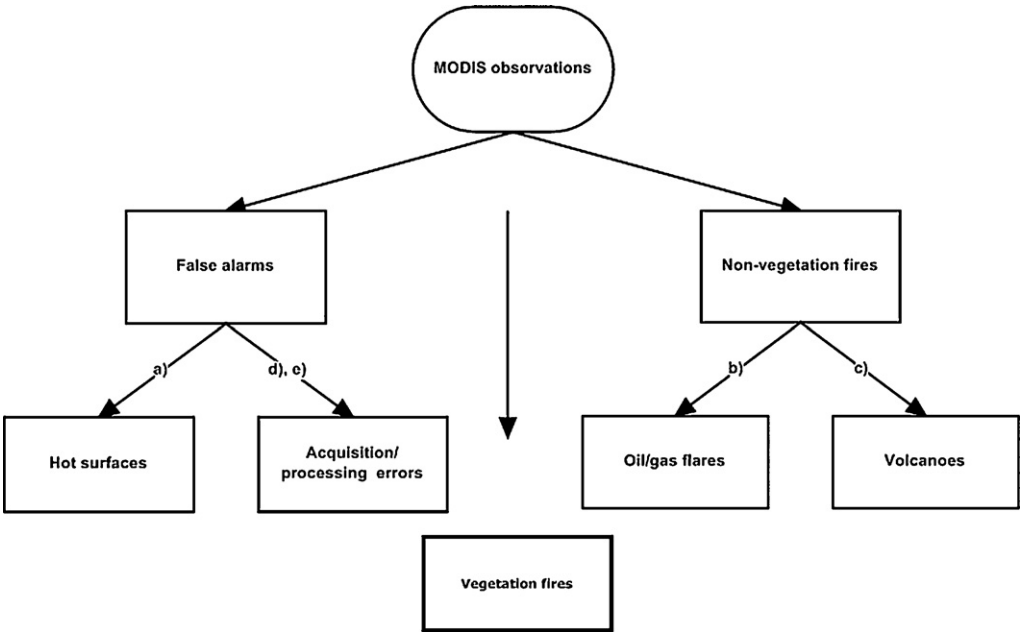

Fig. 1. Hierarchical screening procedure (based on Mota et al., 2006). The parts (a)–(e) are the datasets and index used during the screening procedure. (a) GLC2000, (b) DMSP stable nighttime lights, (c) volcanic activity timing, (d) daily moving average and (e) local Moran index.

non-vegetation fires and false alarms, keeping only vegetation fires in the dataset.

2.2.1.1. First stage screening. The MODIS active fire product (2001–2009) was first screened with the above mentioned combination of ancillary datasets. All the observations falling on GLC2000 classes "bare areas", "natural and artificial water bodies", "snow and ice" and "artificial surfaces and associated areas" were classified as false alarms or non-vegetation fires. Observations (non-vegetation fires) corresponding to gas flares were identified in the gas layer mask based on their circular appearance and lack of coincidence with populated places (Mota et al., 2006). The non-vegetation fires resulting from volcanic activity, were identified through two circular buffers (5 and 10 km radius) plotted around each volcano location, and observations within those buffers were matched against volcanic activity reports. The extent and direction of lava flows were also analyzed. Additionally datasets such as GLC2000 map and Google Earth high resolution images were used to determine whether MODIS observations were generated by volcanic activity, such as pyroclastic eruptions, lava flows, and/or ash plumes, or resulted from actual vegetation fires ignited by volcanic activity. Choice of size of the two buffers was based on analysis of caldera sizes from all the volcanoes. The observations detected in this step were classified as non-vegetation fires.

2.2.1.2. Second stage screening. All the observations that passed the first screening stage were visually screened by identifying very large potentially anomalous, concentrations of observations (in space and/or in time), unlikely to correspond to actual vegetation fires. The difference between daily counts and five-day moving averages was computed to identify atypical temporal clusters in the time-series. This visual/temporal inspection was also performed with exploratory spatial data analysis (ESDA) methods, using local indicators of spatial autocorrelation. Clusters of observations with geometric shapes, as straight lines or arcs were detected and classified as calibration errors (Giglio, 2010). The observations resulting from this screening stage were classified as false alarms. The combination of quantitative, automatic criteria and visual checking complements the first stage screening.

2.2.2. Exploratory spatial data analysis

To quantify spatial heterogeneity at global scale, detect spatial autocorrelation patterns, and identify clusters of similar fire incidence and outliers, an exploratory spatial data analysis (ESDA) of the screened data was performed. The number of fire counts in each 0.5° grid cell was log-transformed ($\log_n$) to reduce the skewness of the original data and improve the performance of ESDA techniques. The new variable was characterized with descriptive statistics and tested for normality with the Kolmogorov–Smirnof test with Lillefors correction. A box and whisker plot was created and the 1.5 Inter-quartile Distance (IQD) rule used to identify distributional outliers. According to this rule, values larger (smaller) than the third (first) quartile + (−)1.5 × IQD were considered outliers (Haining, 1993). To reduce the number of cells to be analyzed and focus on "fire prone cells", an analysis with potentially combustible areas (based on GLC2000 classes with available fuel) and ecoregions of the world (Olson et al., 2001) was performed. The following areas were excluded from further analysis: deserts and small island ecoregions; ecoregions with all grid cells without fire counts or with area smaller than 2500 km^2; all grid cells without fire counts or with less than 10% combustible area. A total of 50 423 half degree cells were kept and used to characterize the spatial pattern of fire at global scale. The global Moran's I statistic measures global (i.e. non-local) spatial autocorrelation and is assessed by testing a null hypothesis of random location, without spatial association (Anselin, 1995; Anselin et al., 2007; Cliff and Ord, 1981). Values of Moran's I larger (smaller) than the expected value $E(I) = -1/(n-1)$, with n as the number of observations, indicate positive-similar (negative-dissimilar) spatial autocorrelation values. However, the global statistic gives a measure of overall clustering and does not reveal the location of clusters or outliers nor the type of spatial correlation that may exist in the data. To overcome these limitations, local indicators of spatial autocorrelation (LISA), such as Local Moran statistic I_i (Anselin, 1995) were used. Anselin (1995) and Anselin et al. (2007) define LISA as an indicator of local spatial patterns and as diagnostics for local instability, i.e. areas where local patterns are not in line with the global indication. Also, as the sum of the I_i for all observations is proportional to the global value of the Moran's I it is possible to decompose Moran's I

into its components, using the Local Moran statistic (I_i), $I_i = (x_i - \mu)\sum W_{ij}(x_j - \mu)$ (Anselin, 1995), where W_{ij} is the element of the spatial weights matrix W corresponding to observation pair (i, j), and represents the component that incorporates "space" (Anselin et al., 2007), denoting the strength of connection between i and j. x_i and x_j are observations for locations i and j, with mean μ. In order to normalize the number of neighbors around a specific location, the spatial weights matrix was row-standardized such that the elements W_{ij} in each row sum to 1. I_i assigns an autocorrelation value to each observation ($\log_n$ fire counts cells). When the data are standardized as $Z_i = (x_i - \mu)/\sigma$, where Z_i is the standardized value of log-transformed fire counts for each cell and σ is the standard deviation, the value of the global Moran's I is equivalent to the slope of a linear regression line of a scatterplot where Z_i is plotted in the x-axis against the mean standardized neighbor value for each location, plotted in the y-axis. This bivariate spatial autocorrelation scatterplot is a graphic tool for detecting local spatial association, also providing a way to categorize the nature of spatial autocorrelation into four types high–high (type 1 – upper right) and low–low (type 3 – lower left) with potential spatial clusters of similar fire frequency, i.e., positive autocorrelation with high or low similar values; high–low (type 2 – lower right) and low–high (type 4 – upper left) with potential spatial clusters of dissimilar values. Positive values of I_i reveal spatial clusters of similar values (either high or low values) and are related with types 1 and 3, while negative values are related with dissimilar values corresponding with types 2 and 4. Thus, the Local Moran statistic in combination with the classification into four types of spatial autocorrelation pattern indicates significant local spatial clusters and facilitates the identification of unusual observations, such as outliers. The significance of Global and Local Moran statistics was evaluated with Monte Carlo randomizations, based on a non-parametric conditional randomization (permutation) approach, where the value x at site i is held fixed and the remaining values are randomly permutated over the other locations in the global dataset (Anselin, 1995). As Local Moran statistics calculated for each grid cell are not independent due overlapping neighborhoods, p-values were corrected with a 0.05 α-level of significance, using the Simes adjustment (Simes, 1986), which is less conservative than the Bonferroni correction.

Three types of regression diagnostics were calculated based on I_i and Moran scatterplot, to detect spatial outliers and analyze their influence on global spatial association: y-discrepancy, leverage and influence measures (Haining, 1994). The first is measured with standardized residuals and detects outliers, observations that are extreme along the dependent variable domain, Y; Leverage (h_i), assessed by the value of the diagonal elements of the hat matrix, is a measure of how far an observation deviates from the mean along the independent variable domain, X. An observation is influential when its exclusion from the dataset determines a large change in the value of the regression coefficients, and can be thought of as combining the effects of the other two diagnostics (Haining, 1994). It is assessed with Cook's distance.

Spatial analysis was performed with Spacestat software vs. 2.0 (Anselin, 1992). The 50 423 standardized, log-transformed fire counts for 2001–2009 were partitioned into four types. The distance range used to define spatial neighborhoods was based on analysis of the correlogram for equal distance bands and was fixed in the 200 km. The neighborhood weighting method used was the inverse distance rank and 999 permutations were employed to build the reference distribution.

Table 1
Annual results of MODIS dataset screening.

Year	Original	Screened	% screened
2001	1 597 241	70 020	4.38
2002	3 349 321	113 672	3.39
2003	4 618 197	141 005	3.05
2004	4 619 040	170 258	3.69
2005	4 670 379	171 415	3.67
2006	4 225 888	160 141	3.79
2007	4 679 841	153 904	3.29
2008	4 369 855	146 789	3.36
2009	4 061 749	134 036	3.30
Mean	4 021 279	1 401 38	3.55

3. Results

3.1. Data screening

The original MODIS dataset has 36 191 511 observations of which 34 930 271 (96.52%) were considered vegetation fires, while 1 261 240 (3.48%) correspond to false alarms or non-vegetation fires. Screening results show an annual percentage of false alarms and non-vegetation fires varying from 3% in 2003 to 4.4% in 2001 (Table 1). Hot bare soils and gas flares are the major sources of false alarms and non-vegetation fires (Table 2).

The years with the most counts were 2007 and 2005, with peaks in August, September and December (Tables 1 and 2). This result is expected because, according to NASA's Goddard Institute for Space Studies (GISS) 2005 and 2007 were two of the hottest years since records began in 1880 (Hansen et al., 2010). The year with fewer counts, excluding 2001 and part of 2002, when one only one sensor was acquiring data, was 2009. Gobron et al. (2010), analyzed a 12-year (1998–2009) time series of Fraction of Absorbed Photosynthetically Active Radiation (FAPAR) and report that 2009 had the strongest negative anomaly for this variable, corresponding to unfavorable conditions for fuel accumulation. Fig. 2 shows the daily time-series of the original MODIS active fire dataset (Fig. 2a), false alarms and non-vegetation fires screened from the original data (Fig. 2b) and the final screened data, containing only vegetation fires (Fig. 2c).

Table 2
Number of observations captured by each filter (observations could be screened by more than one filter).

Year	Landcover				Gas flares	Volcanoes	Calibration errors	Total
	Bare	Water	Artificial	Snow				
2001	23 647	8938	5409	39	32 148	3595	832	74 608
2002	41 641	19 967	8044	17	40 957	7229	0	117 855
2003	42 531	23 878	10 666	40	58 360	7494	0	142 969
2004	60 294	29 391	10 282	16	69 165	6803	705	176 656
2005	57 432	27 147	11 426	164	73 612	7949	0	177 730
2006	55 564	22 758	11 916	42	69 330	6794	0	166 404
2007	48 639	22 485	11 901	102	64 996	7849	0	155 972
2008	42 604	23 679	11 870	64	56 787	6816	6757	148 577
2009	38 430	23 129	10 827	56	52 846	6286	0	131 574
Total	410 782	201 372	92 341	540	518 201	60 815	8294	1 292 345[a]

[a] The total is greater than the number of screened observations due to counting by more than one filter.

The time-series (in particular Fig. 2a and c) shows an increment in fire counts, starting June 2002, justified by the launch of Aqua satellite, while before this date only the MODIS sensor onboard the Terra satellite was acquiring data. The time-series also reveals a seasonal pattern, with a large number of observations during the boreal summer, between July and September, with a peak in August. A secondary peak also occurs between November and February with a maximum in late December and early January. This secondary peak corresponds mainly to savanna fires in northern hemisphere Africa. The year with the most counts is 2007 (in both the original and screened data), with peaks in August–September. The time-series of non-vegetation fires and false alarms (Fig. 2b)

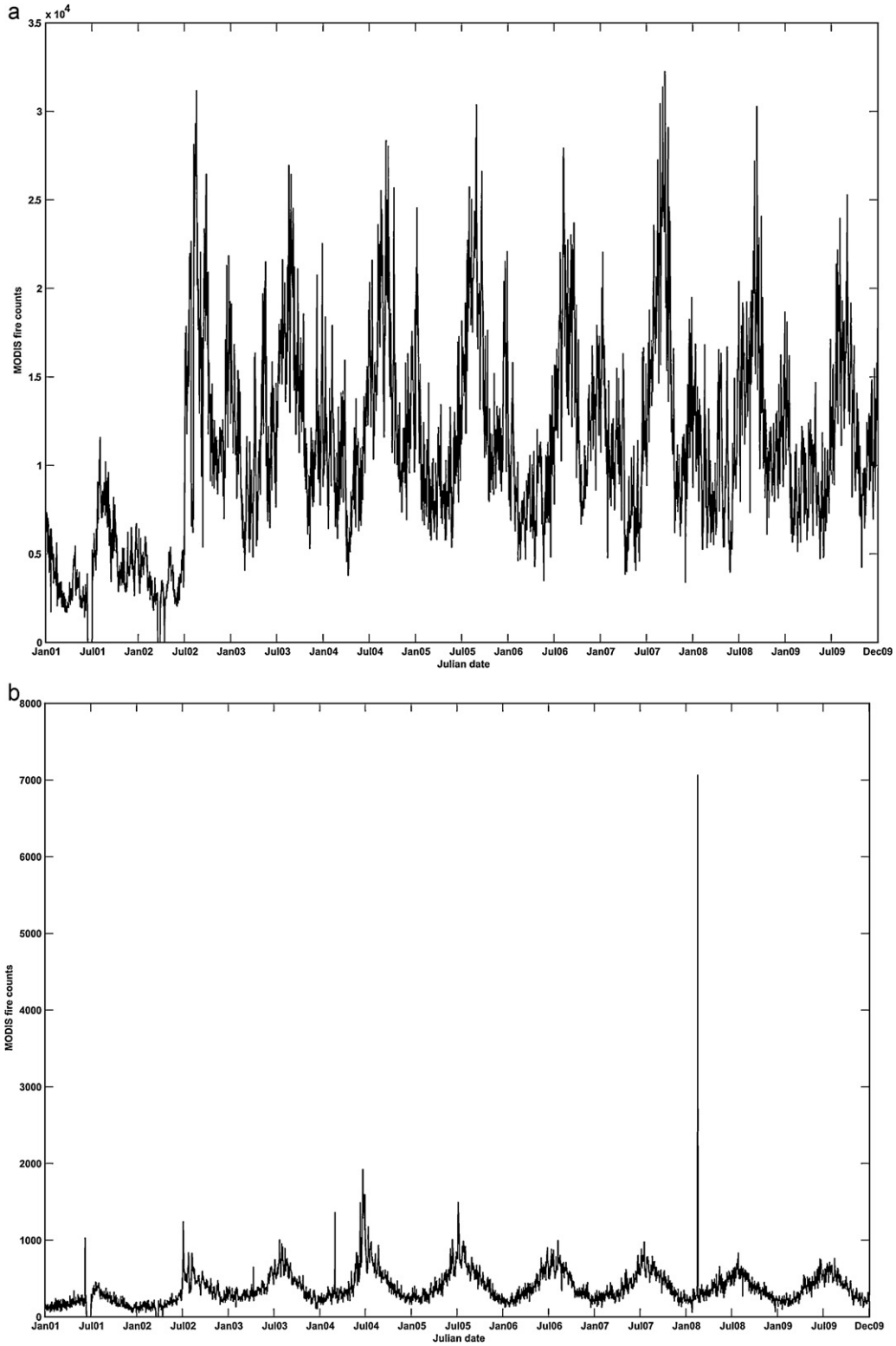

Fig. 2. Daily time-series of (a) original MODIS fire observations, (b) data removed from the original and (c) screened dataset. Only MODIS TERRA data were available from February 2000 to May 2002.

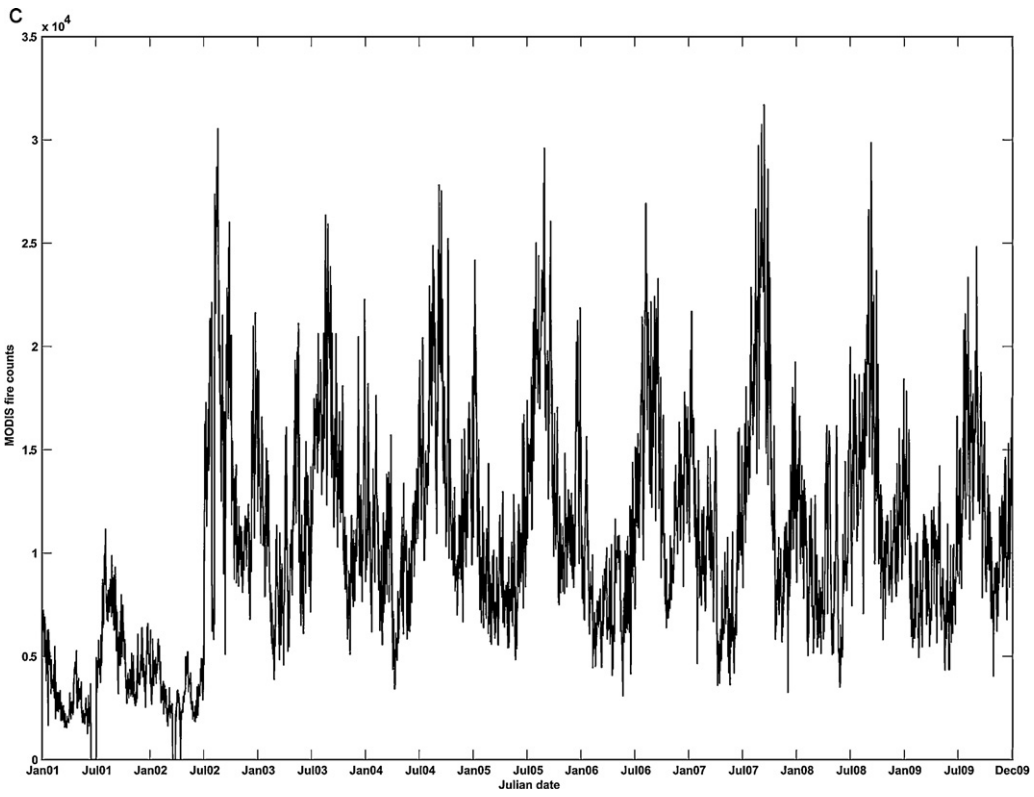

Fig. 2. (*Continued*).

also reveals a seasonal pattern, with a very large spike in February 16, 2008 corresponding to calibration errors. Fig. 3 decomposes the time-series of false alarms and non-vegetation fires into land cover and oil and gas flares filters. Both filters show seasonal patterns with more observations during the boreal summer (note the different scales).

However, while the land cover and oil gas flares time series show a seasonal trend, with more observations during the boreal summer induced by hot land surfaces, the volcanic eruptions time series exhibits a pattern unrelated with climate and with several sporadic spikes, corresponding to large eruptions. The calibration error filter captured three spikes, the largest of which occurred in February 16th, 2008 and corresponds to a cluster of 6757 observations located in northern Russia. The other two spikes are located in Antarctica and northeastern Canada. Fig. 4a–c displays maps of the original MODIS fire data, false alarms and non-vegetation fires, and vegetation fires. Fig. 4a and c is very similar regarding the location of the larger clusters. Fig. 4c displays a geographical fire distribution similar to several previous studies (e.g. Csiszar et al., 2005; Dwyer et al., 2000; Mota et al., 2006), with large clusters located in tropical and sub-tropical zones in the northern and southern hemisphere of Africa, the cerrado savannas of Brazil, savannas and forests in southern Mexico, and tropical savanna in northern Australia. At higher latitudes, Kazakhstan and the northwestern Iberian Peninsula also display high concentration of vegetation fires. The screened observations (Fig. 4b) are mainly concentrated in Kazakhstan and eastern China (landcover filter), Algeria, Libya, Nigeria, Russia and Persian Gulf region (gas flares filter). The land cover filter captured 705 035 observations (55% of all screened observations) with the bare areas class as the most representative, with 410 782 observations (31% of all screened data and 58% of the land cover filtered data).

The gas flares filter, with 518 201 observations removed (40%) and a peak in 2005, shows Iraq (127 499 observations removed), Russia (95 408), Iran (72 575) and Nigeria (40 302) as the countries with the most non-vegetation fires due to oil and gas exploration activities. We analyzed 432 volcanoes which captured 60 815 observations (5% of total screened) for 2001–2009 period, which were not vegetation fires. Volcanoes like Kilauea, in Hawai with 19 985 observations filtered, and African volcanoes like Nyiragongo and Nyamuragira in the Democratic Republic of Congo with a total of 5514 observations, or Erta Ale in Ethiopia with 3989, were those responsible for the larger numbers of observations screened out. Calibration errors were located in Russia, Antarctica and Canada, mainly in 2008. Again, 2005 and 2009 display respectively the largest and smallest number of observations post-screening, for the reasons mentioned above.

3.2. Exploratory spatial data analysis

The 50 423 half degree log-transformed fire counts kept for the period 2001–2009 were used to analyze the spatial structure of fires at global scale. The log-transformation unskewed the data (skewness decreased from 3.690 to −0.022). The Kolmogorov–Smirnof test with Lillefors correction was applied for original fire counts, log-transformed fire counts and log-transformed standardized fire counts and all show that the distributions are non-normal ($p = 0.000$).

The distributional properties of log-transformed fire counts and the geographical distribution of the data classified into quartiles are presented in Table 3 and Fig. 5, respectively. According to the 1.5 IQD rule no distributional outliers were present.

Table 3
Distributional properties of the 50 423 $\log_n$-transformed MODIS fire counts.

Minimum	Maximum	Mean	Std. deviation	Variance
0.000	9.673	3.902	2.840	8.069
Skewness	**Kurtosis**	**1st quartile**	**2nd quartile**	**3rd quartile**
−0.220	−1.245	1.099	4.149	6.267

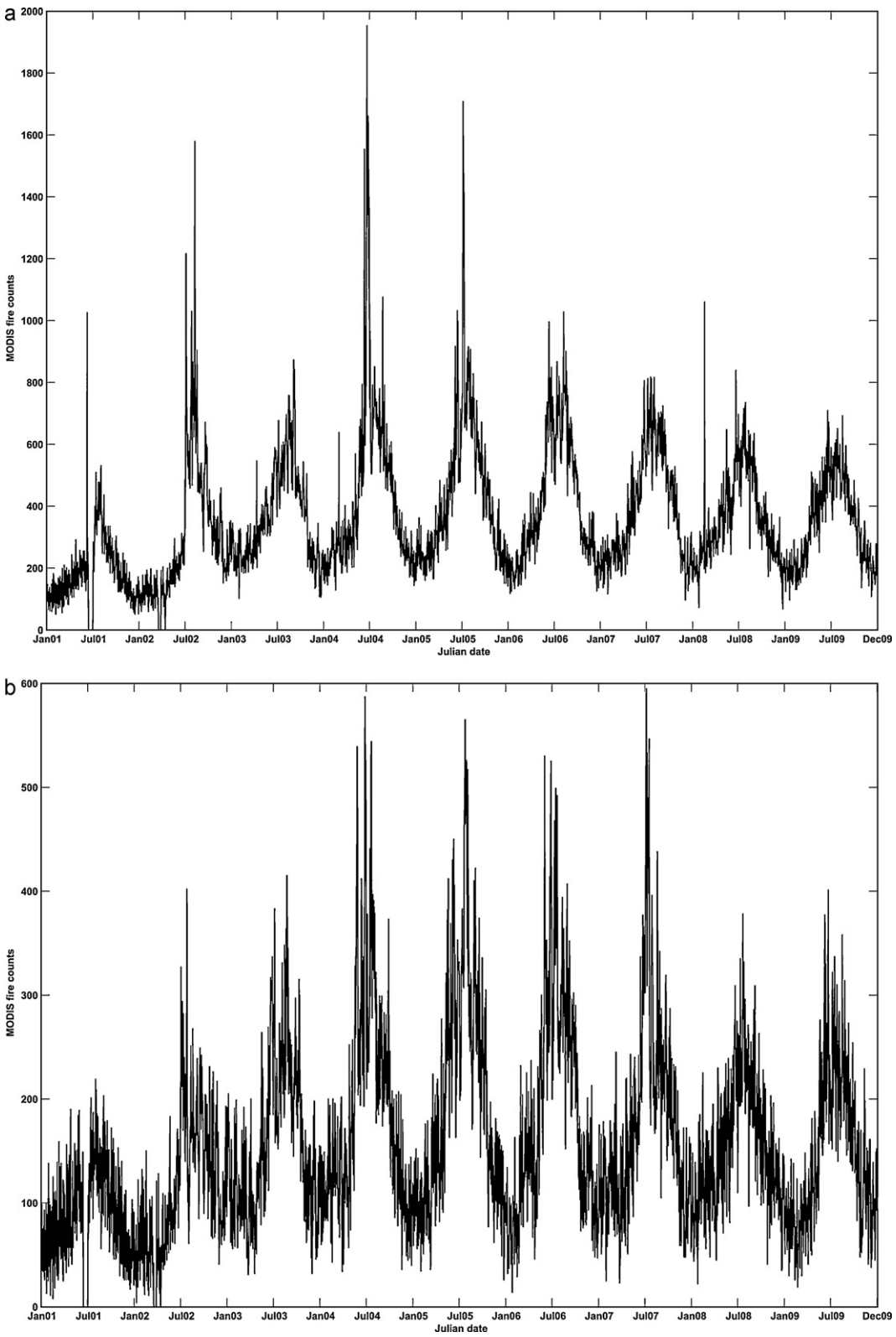

Fig. 3. Daily time-series of original MODIS fire observations removed due each filter: (a) land cover, (b) oil and gas flares. Only MODIS TERRA data were available from February 2000 to May 2002.

3.2.1. Spatial statistics

All calculations were made using standardized log-transformed fire counts. A value of 0.80 ($p = 0.001$) for Global Moran's I was obtained ($\alpha = 0.05$). The expected value for I was −0.00002. Local Moran (I_i) range from −1.82 to 3.90, with a mean of 0.80 (Fig. 6).

Negative values of I_i are located mainly in South America, Canada, Alaska, and Russia. A few cells with negative values are also present in Africa, China, India and Australia. Positive values of Local Moran (I_i) are concentrated in tropical and boreal regions and can be found in all continents. According to the 1.5 IQD rule,

135 I_i spatial outliers were identified, all located in Africa. I_i detected 20 316 cells without significant spatial autocorrelation and 30 107 (60%) spatially autocorrelated cells. From these, 29 269 have a positive sign and 838 a negative sign, indicating correlation of similar and contrasting values, respectively.

3.2.2. Moran scatterplot

The Moran scatterplot (standardized values of the log-transformed fire counts for each cell was plotted against the mean standardized neighbor value for each location) divided the 50 423 cells into four spatial association types (Fig. 7). Out of 30 107 (60%) significantly autocorrelated cells, 14 996 (30%) show spatial clustering of high values (type 1) while 14 273 (28%) display spatial clustering of low values (type 3). 579 cells correspond to type 2 and 259 to type 4. About 20 316 (40%) cells display non-significant autocorrelation ($p > 0.05$). Moran scatterplot regression has a positive slope of 0.80, indicating dominance of positive spatial association and, an r^2 of 0.82.

Fig. 8 displays the geographical distribution of the four types of spatial association.

Regions of positive spatial autocorrelation are colored in gray and yellow (types 1 and 3 respectively) (Fig. 8). Gray regions represents cells of high fire activity, surrounded by similar cells and are located mainly in tropical and subtropical regions, but

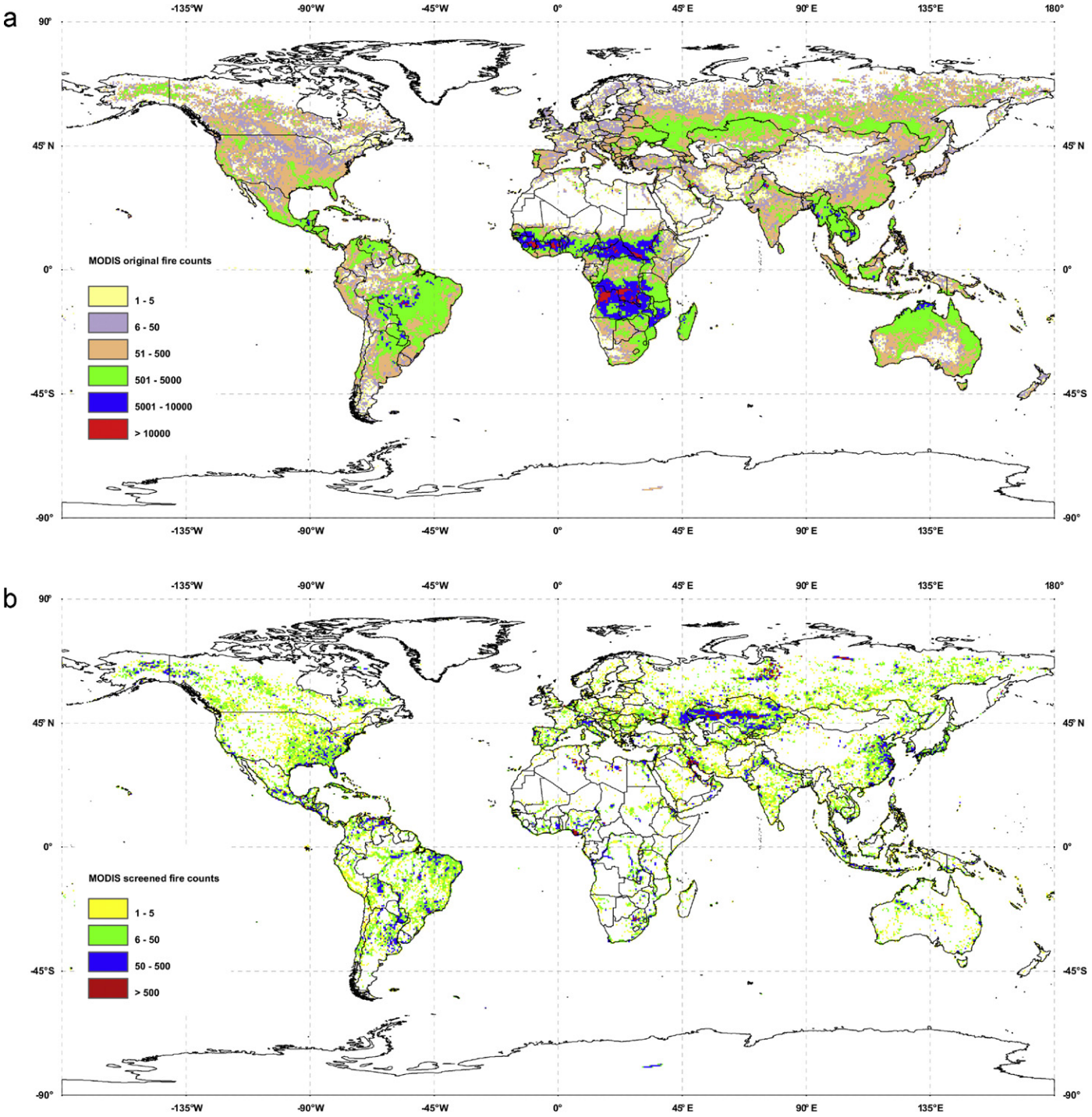

Fig. 4. Global maps (2000–2009) of (a) original MODIS fire counts, (b) removed observations, and (c) vegetation fires data set.

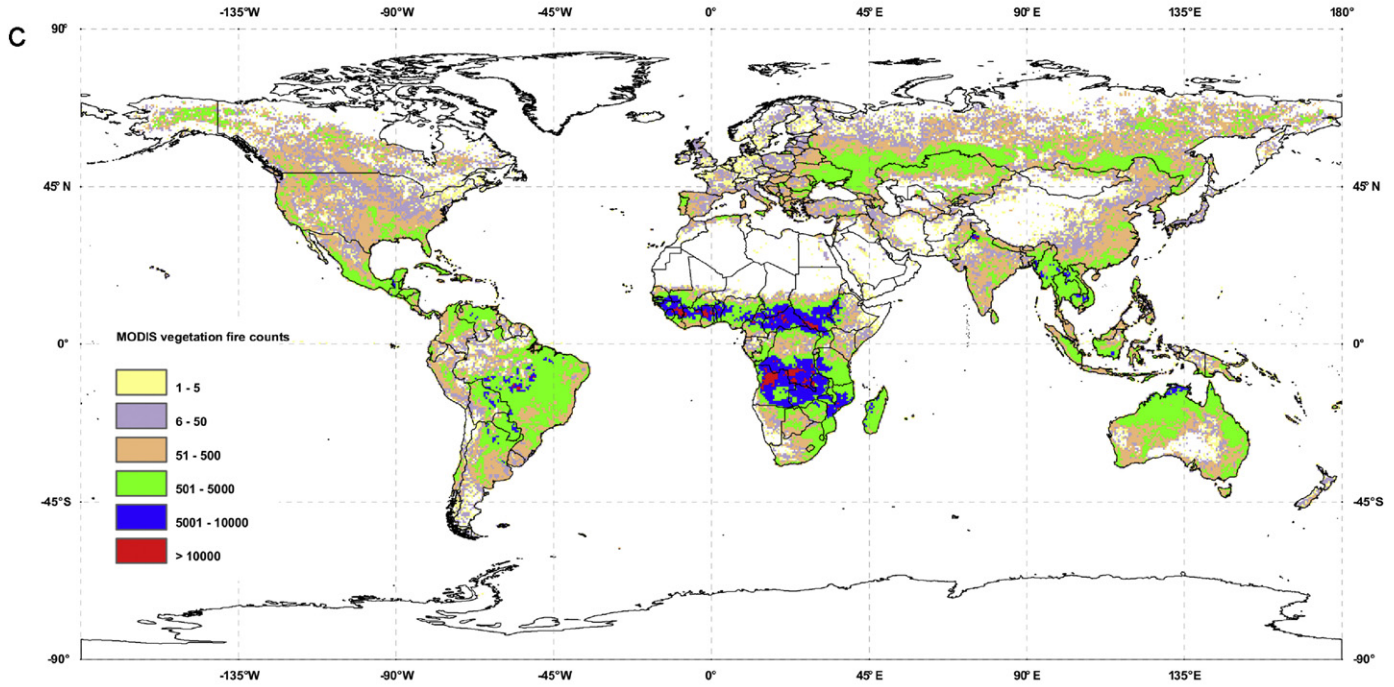

Fig. 4. (*Continued*).

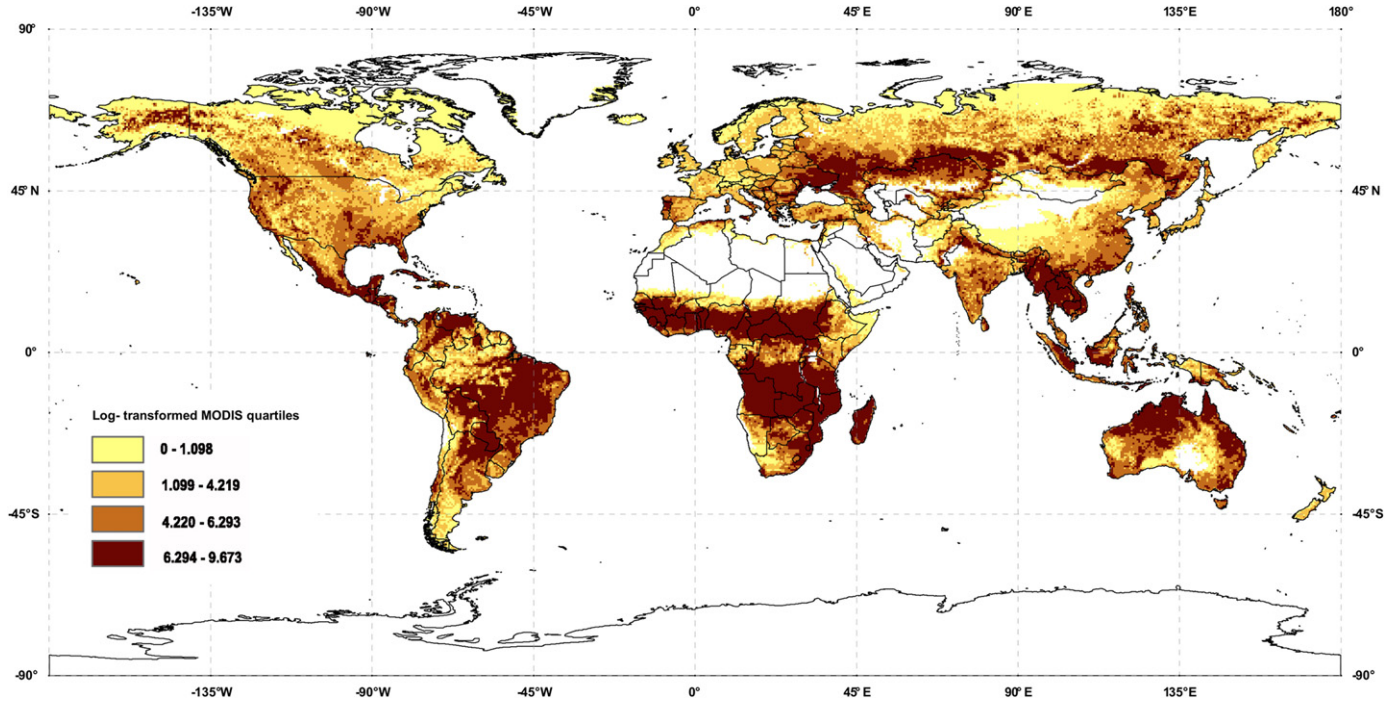

Fig. 5. Log-transformed MODIS fire counts cells quartiles (2001–2009).

also in Alaska, agricultural areas in southeastern USA, and in eastern Europe, extending to northern Kazakhstan. The most positive values are of type 1 (high–high) and are located in tropical zones, such as the sub-Saharan region of northern hemisphere Africa, in the forest savanna-mosaic (Central African Republic and southern Sudan) and in the southern hemisphere tropical woody savannas, especially in Angola miombo woodlands and forest-savanna mosaic. The other positive values of I_i classified as type 3 (low–low), are mainly located in boreal regions, Brazil, Venezuela, and China. The yellow regions represent low fire activity cells located in a low fire activity neighborhood are found mainly in boreal regions, Amazonia, the horn of Africa and Tibet. High–low (type 2) and low–high (type 4) reveal spatial clusters of dissimilar values, i.e. cells with high fire activity in low fire activity neighborhood, and cells with low fire activity in a high fire activity neighborhood. The former are mainly located in Canada, Russia and United States, whereas the latter are found mostly in Brazil and Russia (Fig. 8).

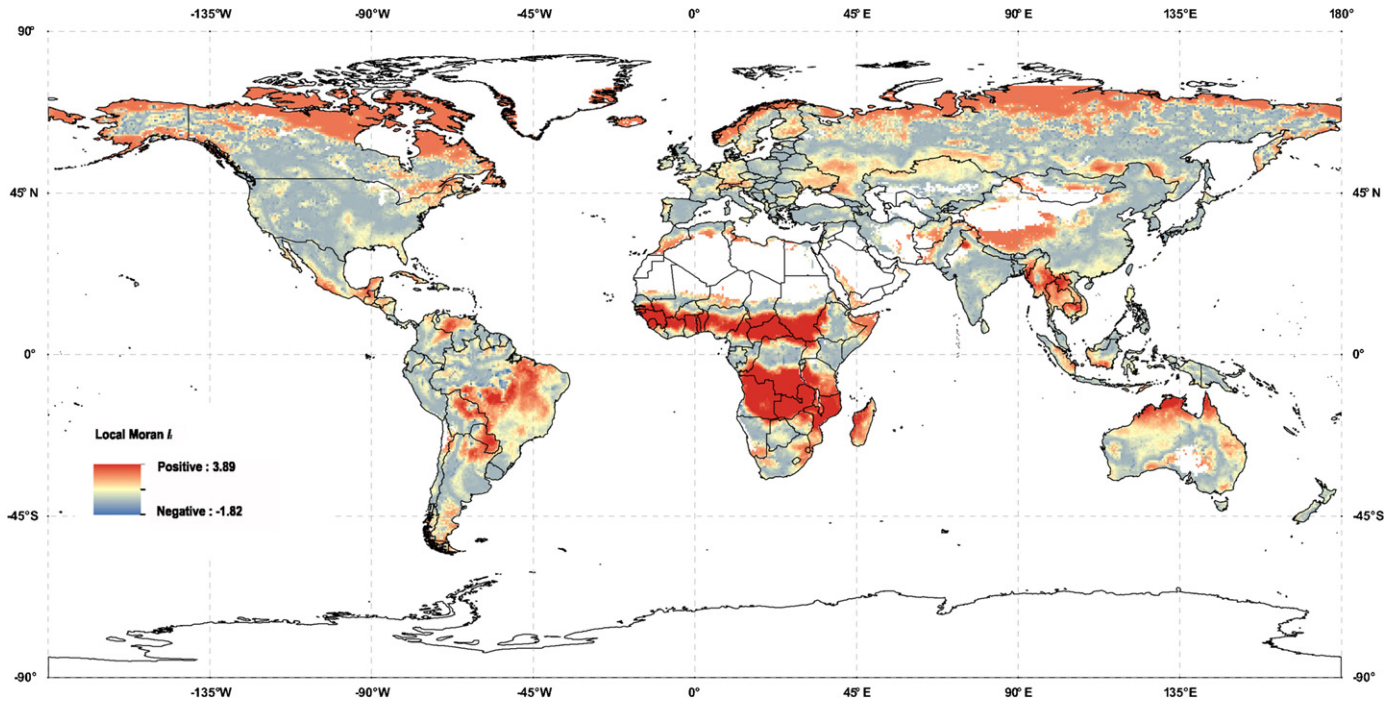

Fig. 6. Geographic distribution of Local Moran, I_i.

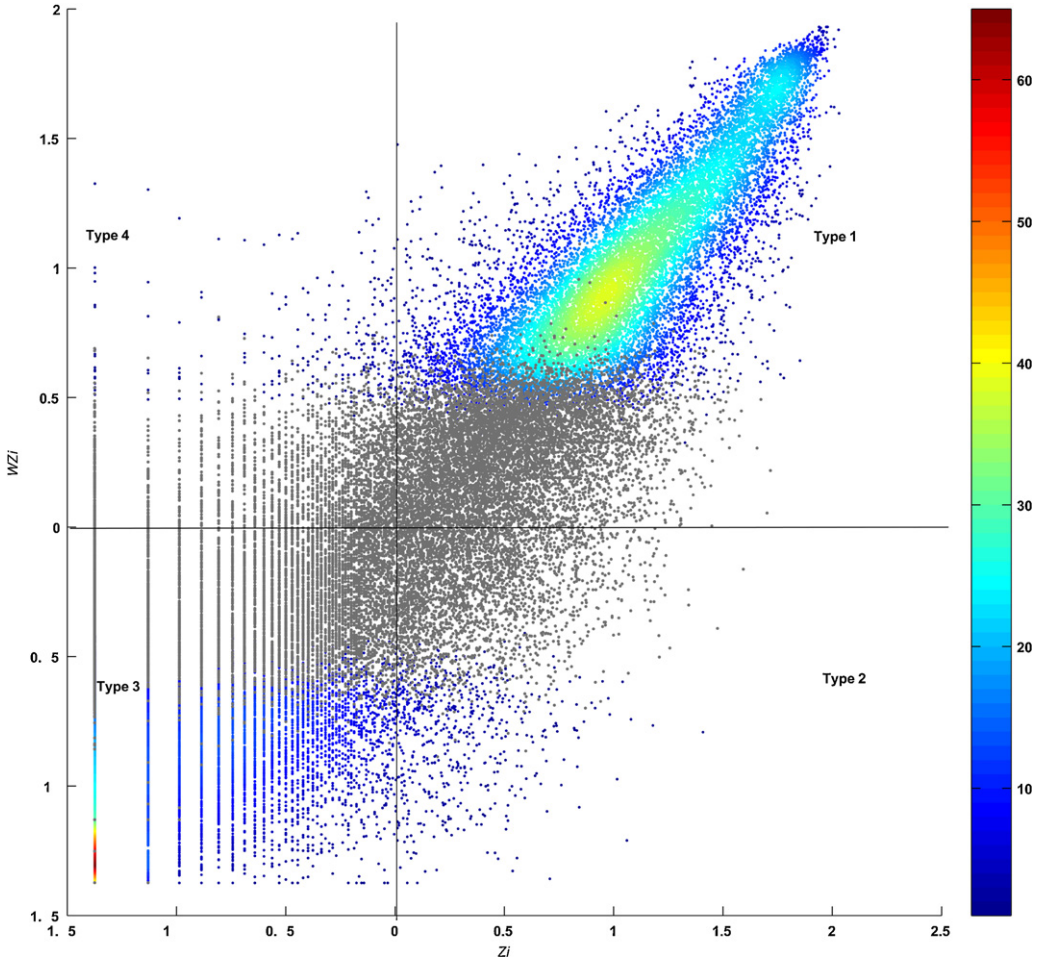

Fig. 7. Moran density scatterplot. Z_i is the standardized value of log-transformed fire counts for each cell and WZ_i is the mean standardized neighborhood value for each cell. Type 1 (high–high, upper right) and type 3 (low–low, lower left) represents potential spatial clusters of similar fire frequency, i.e., positive autocorrelation with high or low similar values respectively; type 2 (high–low, lower right) and type 4 (low–high, upper left) represents potential spatial clusters of dissimilar values. Gray dots are non-significant values.

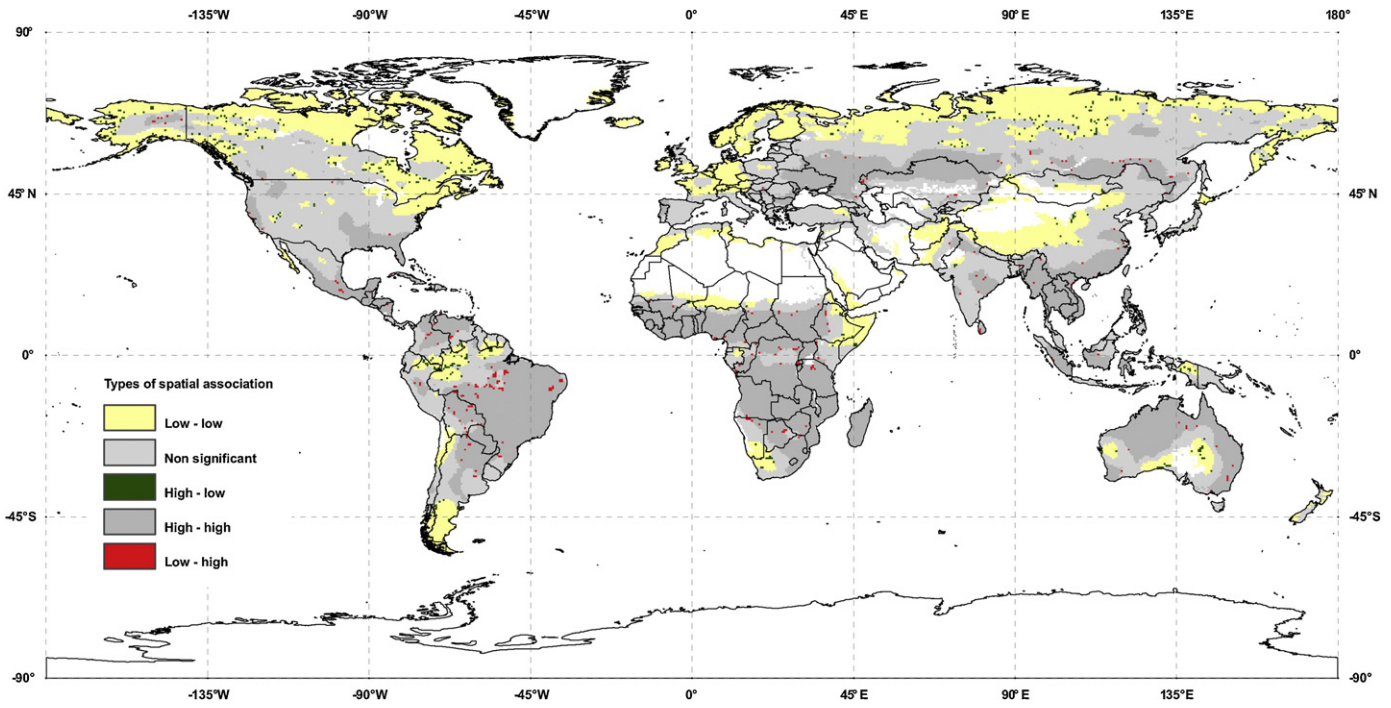

Fig. 8. Geographical distribution of the four types of spatial association, partioned with the Moran scatterplot. The high–low cells are located in Canada, Russia and United States. The low–high cells are mainly located in Brazil, Russia, USA and Canada.

The high–low cell with the most negative I_i value (with 1005 fire counts) is located in Alaska, but that with the most fires is located in Brazil, with 2701 fire counts during the study period. In Russia, the high–low cells with the most fire counts in the period under analysis were located in the Siberian Far East. Brazil is the country with the higher number of low–high cells, with 55, out of a total 259. They are mainly located in protected areas with 34 being located in indigenous areas of the Legal Amazon. The remaining 21 cells occur in four clusters, in the states of Amazonas, Pará, Bahia, and Paraíba. The Russia low–high cells are located near the borders with Kazakhstan, Mongolia and China, where some cells with few fires are surrounded by cells with higher fire activity that are common in those regions.

3.2.3. Regression diagnostics

The ten most extreme observations according to each Moran scatterplot regression diagnostic were analyzed in detail. Fig. 9 displays the spatial distribution of the 30 most extreme observations according to the three types of regression diagnostics (10 for each regression diagnostic): *y*-discrepancy, influence and leverage. Table 4 describes those extreme cells.

Most of these observations are located in the tropical belt, except for three in Alaska. The largest outliers (absolute standardized residuals) are of type 4 (low–high), and type 2 (high–low) and can be found in Brazil, Guatemala, USA (Alaska) and Bolivia. The highest leverage values are of type 1 (high–high) and are located mainly in Africa (Guinea, Sudan and Angola) except for the highest of all, which is located in NW India. The most influential observations, according to Cook's distance, are of type 2 (high–low) for one grid cell in Brazil and one in Alaska, and of type 4 (low–high) for the rest of the cells, located in Brazil, Alaska and Guatemala. Some cells in Brazil, Guatemala, Alaska, Russia and Bangladesh have extreme values, both according to the standardized residuals and Cook's distance diagnostics. For instance, in Brazil the cell with the most extreme residual value is also the most influential one. Due to this identification by more than one diagnostic, the 30 most extreme observations correspond to 22 grid cells, with Brazil (five cells) and Guinea and Angola (four cells each) as the countries with the most extreme values.

4. Discussion

4.1. Data screening

We used a 9-year record of original MCD14ML Collection 5 active fire product, dated from January 2001 through December 2009. The screened fire distribution results are consistent with several global/regional studies, including some performed with data from different sensors. A small percentage of observations (3.5%) were removed from the original dataset, which compares very favorably with the approximately 25% observations found not to be vegetation fires in the ATSR WFA, using a very similar procedure (Mota et al., 2006). The screening procedure highlighted several commission errors caused by a variety of factors, such as hot bare soil surfaces, gas flares, other industrial and urban heat sources, volcanoes, and calibration errors. More than 1 250 000 observations (3.5%) were false alarms or non-vegetation fires, mainly due to hot bare soils. The two-stage screening showed that most false alarms were eliminated with the application of the spatial mask (first stage), while the second stage was much more time consuming identifying anomalies or large clusters concentrated in space and/or time, and unlikely to correspond to actual vegetation fires. All commission errors derived from land cover, gas flares, urban/industrial lights and volcanoes are clustered, either in space, in time, or both, most with a markedly seasonal pattern. As Mota et al. (2006) concluded with ATSR fire data, seasonality in land cover false alarms is mainly induced by hot soil surfaces and, as the observations are captured by more than one filter (not exclusively), the seasonal pattern present in the gas flare observations removed from the dataset results from overlap with those captured with the land cover filter.

4.2. Exploratory spatial data analysis

The Global Moran's *I* statistics provided a good measure of spatial pattern of global fire distribution. A value of $I = 0.80$ revealed

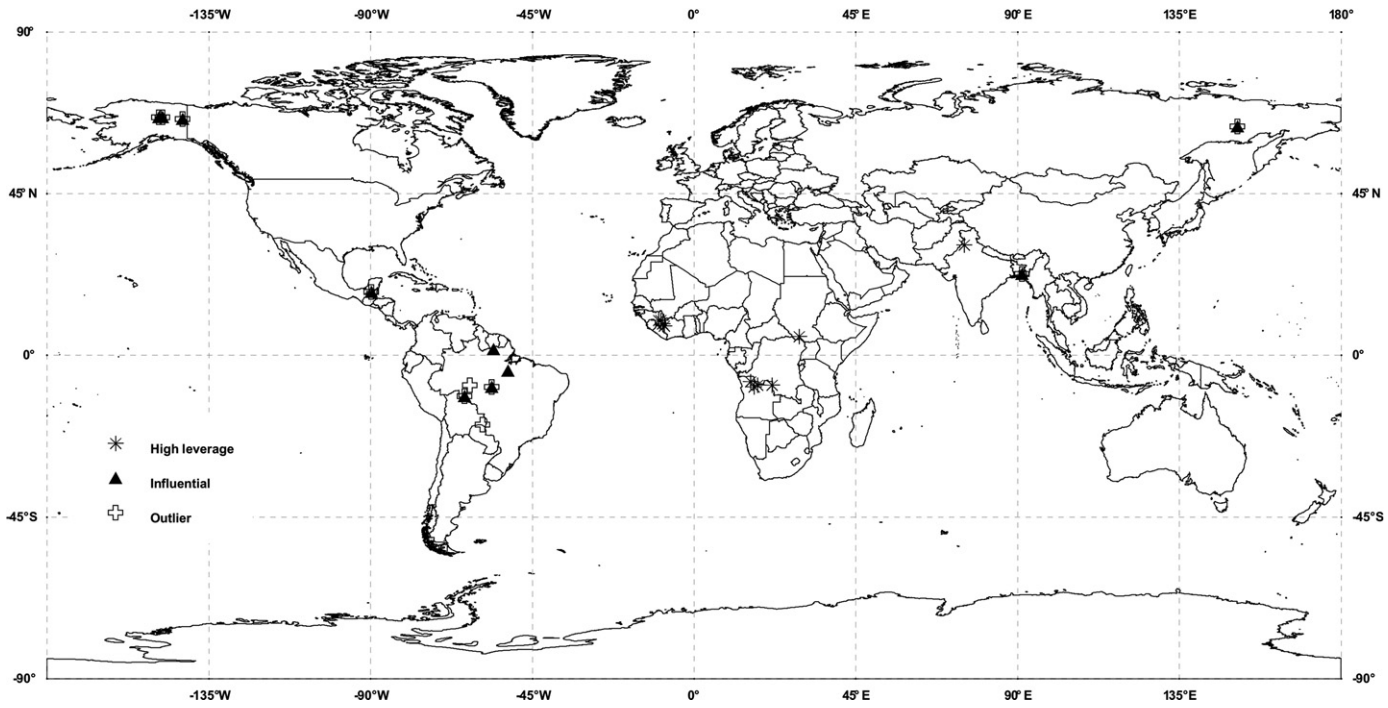

Fig. 9. Geographical distribution of the 10 most extreme observations for each Moran scatterplot regression diagnostic: outliers, high leverage, and influential observations.

strong spatial autocorrelation between fire observations, which was positive at distances up to 200 km. The ESDA detected strong clustering of like values (HH and LL), with the HH clusters primarily located in tropical savannas and temperate agricultural areas, while LL clusters were mostly found in boreal forests. Such strong spatial clustering pattern may indicate the usefulness of developing a regression model with a small number of spatial regimes, to account for likely differences in model parameters in areas associated with these two kinds of cluster. The high spatial autocorrelation values detected, both globally (Moran's *I*), and locally (local Moran's *I*) suggest that it may be worthwhile testing the advantage of developing a spatial lag regression model. Regarding the observations in the LH and HL quadrants of the Moran scatterplot, detailed analysis of the LH cells indicates that it will be appropriate to use an explanatory variable characterizing nature conservation status, at the global scale. The HL cells represent a more difficult problem to model. They typically correspond to large wildfires occurring in areas with fire cycles an order of magnitude longer than the duration of our 9-year dataset, thus representing a temporal sample that is too short to yield stable spatial patterns of fire incidence.

4.3. Regression diagnostics

The spatial distribution of the 30 most extreme observations, according to the Moran scatterplot regression diagnostics is shown in Fig. 9 and Table 4, and discussed below.

4.3.1. Outliers

The largest outlier corresponds to a cell located in the Uru-Eu-Wau-Wau indigenous protected area (11°S, 64°W) in Rondonia, Brazil, an area with around 1 900 000 ha, which was created to protect valuable ecosystems and to preserve a region that represents the transition between Cerrado and Amazonia forests (IBAMA, 2005). The second largest outlier occurs in the Maya Biosphere Reserve, Guatemala (18°N, 90°W), located in the border between Guatemala and Mexico (18°N, 90°W), in a region with three contiguous UNESCO biosphere reserves: the Maya Biosphere Reserve in Guatemala, Calakmul and Montes Azules Biosphere Reserves in southern Mexico. According to the UNESCO Man and Biosphere Programme (MAB), in this Mexican region (more than 3 600 000 ha), one of the biggest areas of tropical forest located north of the Amazon, and the northernmost tropical forest in the Western Hemisphere, efforts have been developed to come up with viable alternatives to slash-and-burn farming. Of the other cells, two are located in Brazil. One is in Pará state (9°S, 56°W), and belongs to a four-cell cluster located at Serra do Cachimbo, in a forest region between two protected areas, located in a military training camp of the Brazilian Air Force. The other cell, located within the Tumucumaque indigenous protected area (2°N, 56°W), was classified as type 2 (high–low) and, from the cells with negative values of I_i, is the one with the most fire observations (2701) during the period of analysis. It coincides with an isolated area of savanna-like vegetation surrounded by moist forests (Tiriyós Savanna), near the border with Surinam. The 2701 fire counts are distributed throughout the entire study period, with a peak in 2004 of around 700 fire observations. Fire, which plays a very important role in the culture of the indigenous population living in the area occurs between September and November, and is used for hunting and pasture renewal (Barbosa and Campos, 2011; Rodrigues et al., 2007). The Bolivia cell (19°S, 59°W) is located in southeastern Bolivia on the borders with Brazil and Paraguay, within in the Otuquis National Park. This protected area is part of one of the largest flood-prone areas in the world – the Pantanal. Although a few agricultural fires may occur within the park, in the surrounding area fire is widely used to clear land for agriculture and ranching, determining the classification of this cell as low–high cell.

Therefore, fire count spatial outlier analysis highlighted the substantial reduction in fire activity in several Amazon protected areas, by contrast with their surroundings, in agreement with Nepstad et al. (2006) suggesting effectiveness of these areas in restricting the use of fire.

The Alaska (USA) cells classified as low–high (66°N, 142°W; 66°N, 148°W; 66°N, 149°W) were adjacent to a group of type 1 (high–high) cells in central-eastern part of the state, where most fire activity occurred in 2004, the worst fire year on record in Alaska (Shulski, 2005). These cells are within Yukon Flats National Wildlife

Table 4
Extreme observations derived from the diagnostic regression. HH – high/high; HL – high/low; LL – low/low; LH – low/high.

Location				Diagnostic regression			Moran scatterplot				Spatial outlier	Observations
ID	Country	Lat., long. (°)	Zone	Outlier	Leverage	Influential	Type 1 (HH)	Type 2 (HL)	Type 3 (LL)	Type 4 (LH)	1.5 IQD rule	
1	Brazil	11S, 64W	Uru-Eu-Wau-Wau	X		X				X		Indigenous protected area[a]
2		9S, 56W	Serra do Cachimbo	X		X				X		Military zone
3		2N, 56W	Tumucumaque	X		X		X				Indigenous protected area[b]
4		4S, 52W	Trincheira Bacajá			X				X		Indigenous protected area[c]
5		5S, 52W				X				X		
6	Guatemala	18N, 90W	Guatemala-Mexico border	X		X				X		UNESCO reserve[d]
7	USA	66N, 142W	Yukon Flats National Wildlife refuge (YFNWR)	X		X				X		Protected area[e]
8		66N, 148W		X		X				X		
9		66N, 149W		X		X				X		
10		61N, 143W	Wrangler St. Elias Nat. Park	X		X		X				2009 Chakina fire[f]
11		63N, 147W	Valdez/Copper River area forestry	X				X				2004 Alphabet Hills fire[g]
12	Bolivia	19S, 59W	Otuquis National Park	X						X		Protected area[h]
13	India	31N, 75W	Punjab		X		X					Agricultural fires[i]
14	Guinea	10N, 10W	Guinea Highlands		X		X				X	Savanna/grassland fires
15		10N, 9W			X		X				X	
16		9N, 9W			X		X				X	
17		8N, 8W			X		X				X	
18	Angola	7S, 16E	Malanje, Lunda and Cuanza provinces		X		X				X	
19		8S, 18E			X		X				X	
20		8S, 22E			X		X				X	
21		9S, 17E			X		X				X	
22	Sudan	5N, 17E	Southwest		X		X				X	

[a] http://pib.socioambiental.org/caracterizacao.php?uf=UF&id_arp=3891.
[b] Rodrigues et al. (2007) and Barbosa and Campos (2011).
[c] http://pib.socioambiental.org/caracterizacao.php?id_arp=3609.
[d] http://www.unesco.org/mab.
[e] Drury and Grissom (2008) and Natcher (2004).
[f] AICC (2009).
[g] Hrobak (2006).
[h] http://www.fcc.org.bo/web/.
[i] Le Page et al. (2010) and Sharma et al. (2010).

Refuge (YFNWR). This is one of the most fire-prone landscapes in Alaska, where fire is allowed as a natural process, under specific environmental conditions depending on values to protect (Natcher, 2004). According to the YFNWR Fire Management Plan summary, the levels defined as critical and full management include zones like villages, native land and with highly valued resources. These zones receive high priority for fire suppression. The cells are in the central part of the refuge where the main villages are located, so fire activity in these cells probably reflects the different levels of intervention used at YFNWR.

The other Alaska cells (61°N, 143°W; 63°N, 147°W) were classified as type 2 (high–low). The first is the high–low cell with the most negative I_i value, and is located within the Wrangell St. Elias National. It corresponds to the Chakina fire of 2009, which burned ca. 23 000 ha. According to the Alaska Interagency Coordination Center (AICC), 2009 was one of the driest and warmest summers on record in southeastern Alaska and had one of the worst wildfire seasons in 50 years. The second cell contains 369 active fires, all observed in 2004 during the Alphabet Hills fire, which lasted for 13 days, burned around 15 000 ha and was part of the Bureau of Land Management (BLM)/Alaska Fire Service (AFS) fuels reduction program to reduced fire danger around communities in the Copper River basin (Hrobak, 2006).

There, outlier analysis highlighted the location of large fires that occurred during the study period. Since this period is very short relatively to the fire cycle of boreal forests, exceptional events stand out clearly.

So, with the exception for the Tumucumaque and Chakina fire events, most of the outliers correspond to protected areas where fire is suppressed and regulated. In fact, wildfires are a major concern in protected area management (Mulongoy and Chape, 2004). Regions like Yukon flats adopted fire managements policies that suppress and exclude fires especially in native owned lands, but around them a “let burn” strategy is the widely adopted (Natcher, 2004).

4.3.2. Leverage

The most extreme values according to the leverage diagnostic were all classified as type 1 (high–high) and are located in Africa (Guinea, Angola and Sudan) with the exception of one cell in Punjab (NW India) near the border with Pakistan. The India cell (31°N, 75°W) contains the second highest number of active fires (of the 30 extreme observations), with 14 066 counts scattered throughout the 9 years, and peaking in 2005. This cell is part of a group of Moran scatterplot high–high cells in Punjab, a region characterized by wheat-rice double crop rotation, where it is common practice

to use of fire for burning agricultural crop residues after the wet season (Le Page et al., 2010; Sharma et al., 2010). All African cells are located in savanna/grassland ecosystems. Five cells are in the northern hemisphere savanna (10°N, 10°W; 10°N, 9°W; 9°N, 9°W; 8°N, 8°W in Guinea and 5°N, 29°E in Sudan) with a large number of fires during the boreal winter (October–March). The Guinea cells are located Guinea Highlands forests. Fires are set intentionally for pasture and farmland clearing. The remaining cells (7°S, 16°E; 8°S, 18°E; 8°S, 22°E; 9°S, 17°E) are located in northern Angola (Malanje, Lunda and Cuanza provinces), the southern part of the Democratic Republic of Congo and in cropland-forest mosaic of Guinea. Fires are set during the dry season (May through September, October), to clear brush, pastures, or old croplands, and also to drive game and livestock.

This diagnostic identifies some of the areas with the highest fire incidence in the world, where fire is regulated for land management purpose

4.3.3. Influence

Cook's distance identifies the cells with the highest influence on the regression coefficients and is the most important regression diagnostic, combining the previous two. The 10 most influential cells are located in the western hemisphere and belong to types 2 (high–low) and 4 (low–high) in the Moran scatterplot. As expected, most were detected by the previous diagnostics, mainly in the absolute standardized residuals (eight out of ten). However two cells (4°S, 52°W; 5°S, 52°W) located in Trincheira Bacajá indigenous protected area (Pará, Brazil), were not included in the 10 extreme values on any the previous diagnostics, but were classified as the 9th and 10th most extreme values according to Cook's distance. These cells (type 4, low–high) coincide with indigenous protected areas in central Pará (Brazil), where restrictions have been imposed on the use of fire. The most influential observation, which was also the largest outlier, is located in the Uru-Eu-Wau-Wau indigenous protected area. These two cells further stress the effectiveness of protected areas in Brazil to contain fire use.

5. Conclusions

The NASA MODIS MCD14ML Collection 5 active fire product for 2001–2009 was screened, prior to performing an ESDA. The global dataset was found to contain 3.5% of observations that are false alarms or non-vegetation fires, and which were eliminated An exploratory spatial data analysis (ESDA) of the screened data revealed strong positive autocorrelation based on global Moran's *I* statistic, stressing the importance of addressing this data feature in the development of spatial regression models of fire presence or abundance Regression scatterplot decomposition of the global Moran's *I*, analysis of its residuals, and local Moran's *I* analysis allowed for the identification and mapping spatial non-stationarity, suggesting heterogeneity in fire–environment relationship across space. Analysis of regression diagnostics highlighted areas with very intensive fire use associated with land management practices, very large fires standing out in regions with long fire cycle, and substantially reduced fire activity in areas with special conservation status.

Acknowledgments

This study was funded by a Ph.D. grant to Duarte Oom (SFRH/BD/47452/2008) from the Foundation for Science and Technology, Ministry for Science and Technology, Portugal. We would like to gratefully acknowledge Minnie Wong (University of Maryland, USA) for providing the MODIS fire dataset, and Alfredo Pereira (INPE, Sao Paulo, Brazil) for help in the interpretation of results.

References

AICC, 2009. Alaska Fire Season 2009, Wildland fire summary and statistics annual report. Alaska Interagency Coordination Center, Predictive Services Center.
Amaral-Turkman, M., Turkman, K., Le Page, Y., Pereira, J.M.C., 2010. Hierarchical space–time models for fire ignition and percentage of land burned by wildfires. Environmental and Ecological Statistics, 1–17.
Anselin, L., 1992. SpaceStat Tutorial: A Workbook for Using SpaceStat in the Analysis of Spatial Data, *Technical Software Series* **S-92-1**. National Center for Geographic Information and Analysis (NCGIA), University of California, Santa Barbara.
Anselin, L., 1995. Local indicators of spatial association – Lisa. Geographical Analysis 27 (2), 93–115.
Anselin, L., Sridharan, S., Gholston, S., 2007. Using exploratory spatial data analysis to leverage social indicator databases: the discovery of interesting patterns. Social Indicators Research 82 (2), 287–309.
Archibald, S., Roy, D.P., van Wilgen, B.W., Scholes, R.J., 2009. What limits fire? An examination of drivers of burnt area in Southern Africa. Global Change Biology 15 (3), 613–630.
Arino, O., Plummer, S., Defrenne, D., 2005. Fire disturbance: the ten years time series of the ATSR World Fire Atlas. In: Lacoste, H. (Ed.), Proceedings of the MERIS (A)ATSR Workshop. September 26–30, ESRIN, Frascati.
Arino, O., Rosaz, J., 1999. 1997 and 1998 world ATSR fire atlas using ERS-2 ATSR-2 data. In: Neuenschwander, L.F., Ryan, K.C., Golberg, G.E. (Eds.), Proceedings of the Joint Fire Science Conference. June 15–17, University of Idaho and the International Association of Wildland Fire, Boise, pp. 177–182.
Barbosa, R.I., Campos, C., 2011. Detection and geographical distribution of clearing areas in the savannas ('lavrado') of Roraima using Google Earth web tool. Journal of Geography and Regional Planning 4 (3), 122–136.
Boschetti, L., Roy, D.P., Justice, C.O., Giglio, L., 2010. Global assessment of the temporal reporting accuracy and precision of the MODIS burned area product. International Journal of Wildland Fire 19 (6), 705–709.
Byun, Y.G., Huh, Y., Yu, K., Kim, Y.I., 2006. Revision of Moran scatterplot approach for more effective forest fire detections. In: World Scientific and Engineering Academy and Society (WSEAS) (Ed.), Proceedings of the 5th WSEAS International Conference on Applied Computer Science. April 16–18, Hangzhou, pp. 951–955.
Chou, Y.H., Minnich, R.A., Chase, R.A., 1993. Mapping probability of fire occurrence in San-Jacinto Mountains, California, USA. Environmental Management 17 (1), 129–140.
Cliff, A.D., Ord, J.K., 1981. Spatial Processes: Models & Applications. Pion, London.
Coluzzi, R., Masini, N., Lanorte, A., Lasaponara, R., 2010. On the estimation of fire severity using satellite ASTER data and spatial autocorrelation statistics. Computational Science and Its Applications-ICCSA 6016, 361–373.
Csiszar, I., Denis, L., Giglio, L., Justice, C.O., Hewson, J., 2005. Global fire activity from two years of MODIS data. International Journal of Wildland Fire 14 (2), 117–130.
De Klerk, H., 2008. A pragmatic assessment of the usefulness of the MODIS (Terra and Aqua) 1-km active fire (MOD14A2 and MYD14A2) products for mapping fires in the fynbos biome. International Journal of Wildland Fire 17 (2), 166–178.
Drury, S., Grissom, P., 2008. Fire history and fire management implications in the Yukon Flats National Wildlife Refuge, interior Alaska. Forest Ecology and Mangement 256, 304–312.
Duncan, B.N., Martin, R.V., Staudt, A.C., Yevich, R., Logan, J.A., 2003. Interannual and seasonal variability of biomass burning emissions constrained by satellite observations. Journal of Geophysical Research 108 (D2), 4100.
Dwyer, E., Pinnock, S., Gregoire, J.M., Pereira, J.M.C., 2000. Global spatial and temporal distribution of vegetation fire as determined from satellite observations. International Journal of Remote Sensing 21 (6–7), 1289–1302.
Elvidge, C.D., Imhoff, M.L., Baugh, K.E., Hobson, V.R., Nelson, I., Safran, J., Dietz, J.B., Tuttle, B.T., 2001. Night-time lights of the world: 1994–1995. ISPRS Journal of Photogrammetry and Remote Sensing 56 (2), 81–99.
Eva, H., Lambin, E.F., 1998. Burnt area mapping in Central Africa using ATSR data. International Journal of Remote Sensing 19 (18), 3473–3497.
Fritz, S., Bartholomé, E., et al., 2003. Harmonisation, Mosaicking and Production of the Global Land Cover 2000 Database (Beta Version). European Commission, Joint Research Centre, EUR 20849 EN.
Giglio, L., 2010. MODIS Collection 4 Active Fire Product User's Guide Version 2.4. Science Systems and Applications, Inc.
Giglio, L., Csiszar, I., Justice, C.O., 2006. Global distribution and seasonality of active fires as observed with the Terra and Aqua Moderate Resolution Imaging Spectroradiometer (MODIS) sensors. Journal of Geophysical Research 111, 1–12.
Giglio, L., Descloitres, J., Justice, C.O., Kaufman, Y.J., 2003. An enhanced contextual fire detection algorithm for MODIS. Remote Sensing of Environment 87 (2–3), 273–282.
Giglio, L., Kendall, J.D., Tucker, C.J., 2000. Remote sensing of fires with the TRMM VIRS. International Journal of Remote Sensing 21 (1), 203–207.
Gobron, N., Belward, A., Pinty, B., Knorr, W., 2010. Monitoring biosphere vegetation 1998–2009. Geophysical Research Letters, 37.
Good, I.J., 1983. Good Thinking: The Foundation of Probability and Its Applications. University of Minnesota Press, Minneapolis.
Haining, R.P., 1993. Spatial Data Analysis in the Social and Environmental Sciences. Cambridge University Press, Cambridge, England/New York.
Haining, R., 1994. Diagnostics for regression modeling in spatial econometrics. Journal of Regional Science 34 (3), 325–341.
Hansen, J., Ruedy, R., Sato, M., Lo, K., 2010. Global surface temperature change. Reviews of Geophysics, 48.

Hawbaker, T.J., Radeloff, V.C., Syphard, A.D., Zhu, Z.L., Stewart, S.I., 2008. Detection rates of the MODIS active fire product in the United States. Remote Sensing of Environment 112 (5), 2656–2664.
Hrobak, J.L., 2006. Alphabet Hills Prescribed Fire (AA30) 2 Year Post-burn Field Monitoring Report. FRAMES Resource Cataloging System (RCS).
IBAMA, 2005. Plano de prevenção aos incêndios florestais Parque Nacional Pacaaás Novos. Ministério do Meio Ambiente, Instituto Brasileiro do Meio Ambiente e Recursos Naturais Renováveis, Campo Novo de Rondônia, Brazil, www.ibama.gov.br/phocadownload/category/44-p?download=2349.pdf (accessed 05.07.10).
Justice, C., Giglio, L., Korontzi, S., Owens, J., Morisette, J., Roy, D., Descloitres, J., Alleaume, S., Petitcolin, F., Kaufman, Y., 2002. The MODIS fire products. Remote Sensing of Environment 83 (1–2), 244–262.
Kasischke, E.S., Hewson, J.H., Stocks, B., van der Werf, G., Randerson, J., 2003. The use of ATSR active fire counts for estimating relative patterns of biomass burning – a study from the boreal forest region. Geophysical Research Letters 30 (18).
Krawchuk, M.A., Moritz, M.A., Parisien, M.A., Van Dorn, J., Hayhoe, K., 2009. Global pyrogeography: the current and future distribution of wildfire. PLoS One 4 (4).
Le Page, Y., Oom, D., Silva, J., Jönsson, P., Pereira, J., 2010. Seasonality of vegetation fires as modified by human action: observing the deviation from eco climatic fire regimes. Global Ecology and Biogeography 19 (4), 575–588.
Morisette, J.T., Giglio, L., Csiszar, I., Justice, C.O., 2005a. Validation of the MODIS active fire product over Southern Africa with ASTER data. International Journal of Remote Sensing 26 (19), 4239–4264.
Morisette, J.T., Giglio, L., Csiszar, I., Setzer, A., Schroeder, W., Morton, D., Justice, C.O., 2005b. Validation of MODIS active fire detection products derived from two algorithms. Earth Interactions, 9.
Mota, B.W., Pereira, J.M.C., Oom, D., Vasconcelos, M.J.P., Schultz, M., 2006. Screening the ESA ATSR-2 World Fire Atlas (1997–2002). Atmospheric Chemistry and Physics 6, 1409–1424.
Mulongoy, J.K., Chape, S., 2004. Protected Areas and biodiversity: An Overview of Key Issues. CBD Secretariat/UNEP – WCMC, Montreal, Canada/Cambridge, UK.
Natcher, D.C., 2004. Implications of fire policy on native land use in the Yukon Flats, Alaska. Human Ecology 32 (4), 421–441.
Nepstad, D., Schwartzman, S., et al., 2006. Inhibition of Amazon deforestation and fire by parks and indigenous lands. Conservation Biology 20, 65–73.
Olson, D.M., Dinerstein, E., et al., 2001. Terrestrial ecoregions of the worlds: a new map of life on Earth. Bioscience 51, 933–938.
Oom, D., 2008. Classificação global de fogos de vegetação com base em padrões espaciais, temporais, e de uso/coberto do solo para o período entre 1996 e 2006. MSc Dissertation. Technical University of Lisbon.
Pereira, J.M.C., 2003. Remote sensing of burned areas in tropical savannas. International Journal of Wildland Fire 12 (3–4), 259–270.
Pereira, J.M.C., Carreiras, J.M.B., Perestrello de Vasconcelos, M.J., 1998. Exploratory data analysis of the spatial distribution of wildfires in Portugal, 1980–1989. Geographical Systems 5, 355–390.
Pereira, J.M.C., Mota, B., Privette, J.L., Caylor, K.K., Silva, J.M.N., Sa, A.C.L., Ni-Meister, W., 2004. A simulation analysis of the detectability of understory burns in miombo woodlands. Remote Sensing of Environment 93 (3), 296–310.
Prins, E.M., Menzel, W., 1992. Geostationary satellite detection of biomass burning in South America. International Journal of Remote Sensing 13 (15), 2783–2799.
Rodrigues, C.A.G., Hott, M.C., Miranda, E.E., Oshiro, O.T., 2007. Análise da savana e queimadas no Parque Indígena de Tumucumaque (PA) através de imagens de satélite Landsat. In: INPE (Ed.), Anais XIII Simpósio Brasileiro de Sensoriamento Remoto. Florianópolis, Brazil, pp. 4195–4202.
Sá, A.C.L., Pereira, J.M.C., Charlton, M.E., Mota, B., Barbosa, P.M., Stewart Fotheringham, A., 2011. The pyrogeography of sub-Saharan Africa: a study of the spatial non-stationarity of fire–environment relationships using GWR. Journal of Geographical Systems 13 (3), 227–248.
Schroeder, W., Prins, E., Giglio, L., Csiszar, I., Schmidt, C., Morisette, J., Morton, D., 2008a. Validation of GOES and MODIS active fire detection products using ASTER and ETM plus data. Remote Sensing of Environment 112 (5), 2711–2726.
Schroeder, W., Ruminski, M., Csiszar, I., Giglio, L., Prins, E., Schmidt, C., Morisette, J., 2008b. Validation analyses of an operational fire monitoring product: the hazard mapping system. International Journal of Remote Sensing 29 (20), 6059–6066.
Schultz, M.G., 2002. On the use of ATSR fire count data to estimate the seasonal and interannual variability of vegetation fire emissions. Atmospheric Chemistry and Physics 2, 387–395.
Sharma, A.R., Kharol, S.K., Badarinath, K.V.S., Singh, D., 2010. Impact of agriculture crop residue burning on atmospheric aerosol loading – a study over Punjab State, India. Annales Geophysicae 28 (2), 367–379.
Shulski, M., 2005. Alaska's exceptional 2004 fire season. In: Sixth Symposium on Fire and Forest Meteorology, Cabmore, AB, Canada.
Siljander, M., 2009. Predictive fire occurrence modelling to improve burned area estimation at a regional scale: a case study in East Caprivi, Namibia. International Journal of Applied Earth Observation and Geoinformation 11 (6), 380–393.
Simes, R.J., 1986. An improved Bonferroni procedure for multiple tests of significance. Biometrika 73 (3), 751–754.
Stroppiana, D., Pinnock, S., Gregoire, J.M., 2000. The global fire product: daily fire occurrence from April 1992 to December 1993 derived from NOAA AVHRR data. International Journal of Remote Sensing 21 (6–7), 1279–1288.
Tukey, J.W., 1977. Exploratory Data Analysis. Addison-Wesley, Reading, MA.